Journal of Structural Geology 33 (2011) 1158–1168

Contents lists available at ScienceDirect

Journal of Structural Geology

journal homepage: www.elsevier.com/locate/jsg

Incremental fold test for paleostress analysis using the Hough transform inverse method

Satoshi Tonai [a,*], Katsushi Sato [a], Juichiro Ashi [b]

[a] Division of Earth and Planetary Sciences, Graduate School of Science, Kyoto University, Sakyo-ku, Kyoto 606-8502, Japan
[b] Atmosphere and Ocean Research Institute, The University of Tokyo, Kashiwa, Chiba 277-8564, Japan

ARTICLE INFO

Article history:
Received 4 February 2011
Received in revised form
11 May 2011
Accepted 14 May 2011
Available online 23 May 2011

Keywords:
Stress tensor inversion
Fold test
Fault-slip analysis
Kyushu
Japan

ABSTRACT

An incremental fold test method for the paleostress inversion of a fault-slip dataset obtained from folded sedimentary rock is proposed. The method provides not only the orientations of the three principal stress axes and the stress ratio, but also the relative timing of folding and faulting. The method is based on the stepwise backtilting of strata. Significant stresses are identified by simply comparing peak values of total goodness of fit for the paleostress inversion technique and the stress differences among peaks detected from each step of backtilting of a fault-slip dataset. To assess its validity, the method is applied to artificial fault-slip datasets generated with hypothetical histories of folding, and faulting and with known paleostresses. The proposed method successfully recovers the artificial stress tensors and the relative ages of folding and faulting. Second, the method is applied to a natural fault-slip dataset obtained for Eocene sedimentary strata in Kyushu, southwest Japan, folded around NE–SW-trending axes in the Miocene. The analysis yields three significant paleostresses: a normal-faulting stress that occurred before folding, and two syn-folding stresses, indicating the existence of a spatially and temporally varying stress field during folding.

1. Introduction

Paleostress inversion for folded rock masses requires great care because the orientation of fault-slip data is inevitably changed by tilting of the rock mass after faulting (Fig. 1). Such rotated data may produce misleading results if the influence of tilting is ignored. To address the problem, it is necessary to obtain the original attitudes of fault-slip data prior to tilting of the rock mass. In addition, fault-slip datasets are commonly heterogeneous, reflecting fault activity under various stress regimes and at different times. Thus, to accurately reconstruct the stress history, it is necessary to determine the relative timing of tilting and fault activity.

To identify multiple stress regimes that occurred at different times, previous studies have classified minor faults into homogeneous subsets at the outcrop scale based on their apparent relative ages (e.g., Angelier et al., 1986; Choi et al., 2001; Viola et al., 2009). Some of the features of minor faults are useful in distinguishing different fault sets, including the age of the rocks affected by a certain deformation event (Choi et al., 2001; Vandycke and Bergerat, 2001; Yamaji, 2003), the characteristics of syn-sedimentary faults (e.g., fault drag) (Choi et al., 2001; Vandycke and Bergerat, 2001), the geometrical relationships between geological structures (Angelier et al., 1986; Vandycke and Bergerat, 2001), the occurrence of multiple striations on a single fault plane (Rossetti et al., 2000; Storti et al., 2001), and the characteristics and mineralogy of veins (Choi et al., 2001; Viola et al., 2009). Unfortunately, these criteria are not always applicable because of a lack of suitable outcrop data. Furthermore, to determine temporal relationship between folding and faulting, it is often assumed that one of the three principal stress axes is vertical and that the other two are horizontal; however, this is not always the case, particularly for folded rock masses (Couples et al., 1998).

Yamaji et al. (2005) proposed a numerical technique for deciphering multiple paleostresses from a fault-slip dataset obtained for a folded rock mass. Several numerical techniques have been developed to separate stress tensors from heterogeneous fault-slip datasets (Etchecopar et al., 1981; Armijo et al., 1982; Nemcok and Lisle, 1995; Yamaji, 2000; Shan et al., 2004; Yamaji et al., 2006; Žalohar and Vrabec, 2007). Yamaji et al. (2005) applied incremental backtilting to the multiple-inverse method (Yamaji, 2000), for which the underlying concept is inspired by the 'bedding tilt test' or the 'fold test' of paleomagnetism, as used to recover the

* Corresponding author. Present address: National Institute of Advanced Industrial Science and Technology (AIST), Geological Survey of Japan, Tsukuba, Ibaraki 305-8567, Japan.
E-mail address: s-tonai@aist.go.jp (S. Tonai).

0191-8141/$ – see front matter © 2011 Elsevier Ltd. All rights reserved.
doi:10.1016/j.jsg.2011.05.005

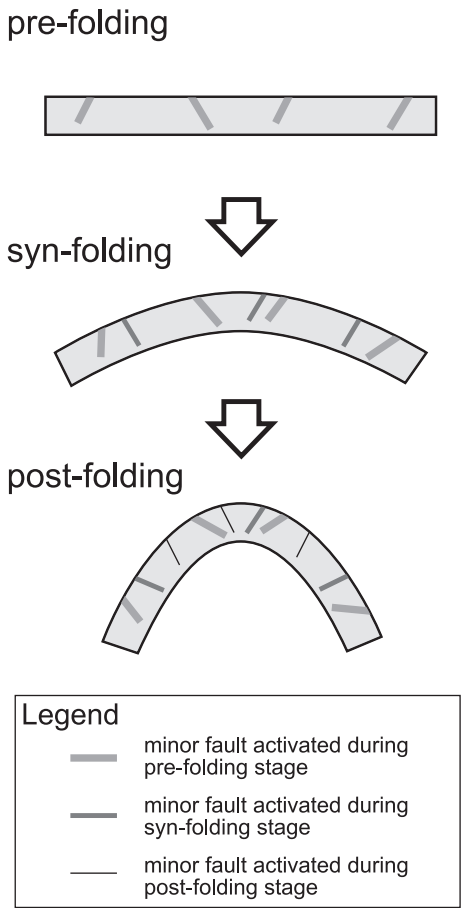

Fig. 1. Minor faults activated during the pre-, syn-, and post-folding stages. Note the rotation of early faults during folding.

initial paleomagnetic vectors (Graham, 1949; Butler, 1992). In their technique, the paleostress is inferred for a significantly tilted rock mass based on the degree of concentration of clusters defined by stress tensors in a stress space. However, their technique did not take into account the goodness of fit of the detected paleostresses to the fault-slip dataset. In addition, their technique cannot be applied to other paleostress inversion methods, except for the multiple-inverse method.

In this study, we applied the incremental fold test for paleostress inversion using the Hough transform (Yamaji et al., 2006). This inversion technique is herein referred to as HIM (Hough transform Inverse Method). In the following sections, the testing method is explained and then applied to artificial and natural datasets. The natural data were collected from a Middle Eocene sedimentary sequence in southwest Japan, which was folded in the Early Miocene.

2. Testing method

2.1. Basic outline of HIM

The application of HIM involves evaluating the goodness of fit of reduced stress tensors to fault-slip data in the parameter space, as proposed originally by Fry (1999, 2001) and subsequently modified by Sato and Yamaji (2006a).

A reduced stress tensor has four independent variables: the orientations of the principal stresses (σ_1, σ_2 and σ_3) and the stress ratio $\Phi = (\sigma_2 - \sigma_3)/(\sigma_1 - \sigma_3)$. The principal stresses σ_1, σ_2, and σ_3, where $\sigma_1 \geq \sigma_2 \geq \sigma_3$, are described following the geological convention that compression is positive. In the parameter space for stress inversion, a reduced stress tensor has a one-to-one correspondence with a five-dimensional unit vector $\vec{\sigma}$ called the σ-vector (Sato and Yamaji, 2006a). Hereafter, $\vec{\sigma}$ denotes a reduced stress tensor and is regarded as a point on a five-dimensional unit sphere S_5.

The goodness of fit of a reduced stress tensor to a fault-slip datum is evaluated using a method that employs d, the angular misfit between observed and calculated slip directions on the fault. The calculated slip directions are evaluated by the Wallace–Bott hypothesis, which assumes that fault slip occurs in the direction of the resolved shear stress exerted on the fault surface (Wallace, 1951; Bott, 1959). The goodness of fit for all possible reduced stress tensors, based on their d values, is evaluated at uniformly distributed grid points on S_5 (Sato and Yamaji, 2006b).

Let $f^{(k)}(\vec{\sigma})$ be the fitness function on S_5 for the kth fault-slip datum. Then, the fitness functions for all fault-slip data are superposed,

$$F(\vec{\sigma}) = \sum_{k=1}^{N} f^{(k)}(\vec{\sigma}), \tag{1}$$

where N is the number of fault-slip data. This total goodness of fit $F(\vec{\sigma})$ is the objective function of HIM. Grid points which give peaks of $F(\vec{\sigma})$ are regarded as potential solutions of the stress inversion technique (Yamaji et al., 2006).

The fitness functions are differently defined for three types of fault-slip data (Appendix. A). A fault-slip datum which is composed of fault orientation, slip orientation, and sense of slip is ideal and called a full datum (Sato, 2006); however, it is often difficult to identify slip orientations or slip senses from natural faults (e.g., Lisle et al., 2001; Yamaji, 2003). A fault-slip datum for which the sense of slip (slip orientation) cannot be observed is called a line-only (sense-only) datum (Sato, 2006). Line-only and sense-only data place looser constraints on reduced stress tensors and are interpreted into a wider distribution of fitness functions on S_5 (Sato, 2006). Consequently, the contribution of these data to $F(\vec{\sigma})$ is defined to be smaller than that of full data (Sato, 2006).

To detect peaks, $F(\vec{\sigma})$ of the grid points is compared with that of neighboring grid points. If the value for a given datum is the greatest among those of its neighbors, a peak is identified at the

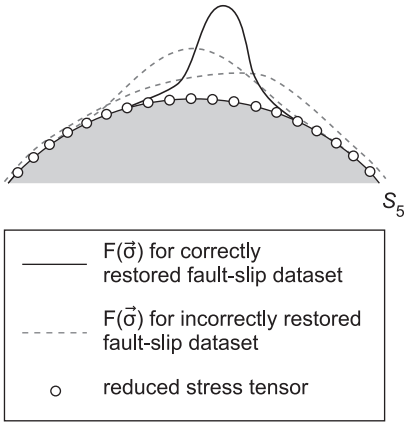

Fig. 2. Schematic figure showing the concept of the incremental fold test proposed in this study. In the five-dimensional parameter space, the goodness of fit is evaluated at uniformly spaced grid points corresponding to reduced stress tensors (open circles) on the unit sphere S_5. The goodness of fit distributions is superposed to give the total goodness of fit $F(\vec{\sigma})$ for all fault-slip data, for which the peaks are possible solutions.

grid point. The range of values for neighboring data is defined by the "angular stress distance" (Yamaji and Sato, 2006), which is a measure of the difference between reduced stress tensors, expressed as the angular distance between corresponding points on S_5, with values ranging from 0° to 180° (Yamaji and Sato, 2006). The distance has been found to approximate the averaged mismatch of shear stress directions on randomly oriented fault planes exerted by two reduced stress tensors (Yamaji and Sato, 2006). In this paper, we set the angular stress distance to 47°, which corresponds to a stress difference (Orife and Lisle, 2003) of 0.8, as the range of neighbor-comparison.

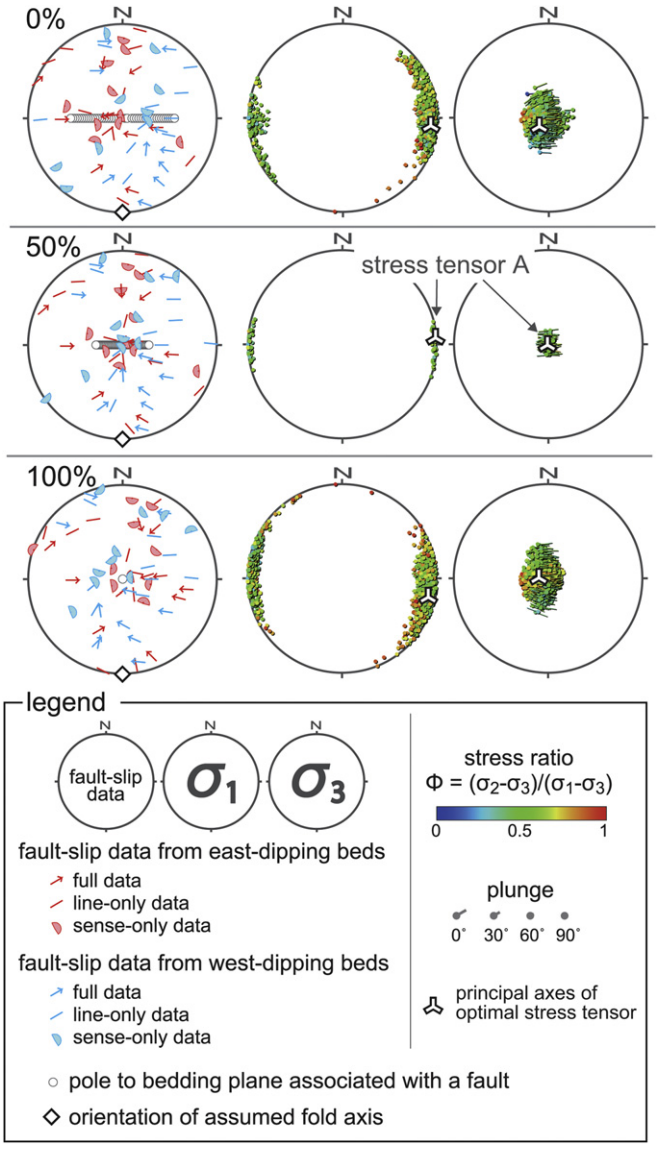

Fig. 3. Stereograms showing the artificial fault-slip dataset (left-hand column) and the results of HIM (center and right-hand columns) for Case 1. Lower-hemisphere, equal-area projections. Left-hand column: open circles indicate the orientations of strata from which the fault-slip data were collected, and the fault-slip data are shown as tangent–lineation diagrams (Twiss and Gefell, 1990). Center and right-hand columns: reduced stress tensors with a relatively high value of $F(\vec{\sigma})$ for the datasets. In the center (right-hand) column, the orientations of σ_1 (σ_3) axes are plotted as small circles, and the lengths and directions of attached bars indicate the orientations of σ_3 (σ_1) axes, as if there were small stereograms around the small circles. The colors of the symbols indicate the value of the stress ratio. Percentage values shown in the upper left corner of each panel indicate the amount of backtilting. (For interpretation of the references to color in this figure legend, the reader is referred to the web version of this article.)

2.2. Incremental fold test

The proposed incremental fold test is based on the following assumptions. The peaks in $F(\vec{\sigma})$ for a fault-slip dataset for which the attitudes have been correctly restored to those at the time when the faults were activated, are expected to be higher than those obtained for incorrectly restored dataset (Fig. 2). The potential stress solutions derived from incorrectly restored datasets not only have lower values of $F(\vec{\sigma})$, but also deviate from the true reduced stress tensors (Fig. 2).

In this study, we assume that all fold limbs are tilted at the same rate; i.e., if the present and past dips of a bed in a limb are D_t and D, respectively, the ratio D/D_t is assumed to be spatially uniform within the area of interest. Below, the parameter $100(1 - D/D_t)\%$ is referred to as the amount of backtilting.

The procedure followed in the proposed method is as follows. First, from a fault-slip dataset obtained from both limbs of folds, we prepare several rotated datasets by backtilting the fault-slip data until the bedding planes are horizontal. The rotation axes for backtilting are assumed to be parallel to the strikes of the strata around the faults. Second, each rotated fault-slip dataset is analyzed by HIM to identify the peaks of $F(\vec{\sigma})$. Then, to find the maxima of peaks corresponding to the correctly restored fault-slip datasets, the peak values of goodness of fit and the angular stress distances of peaks are compared for the different the backtilting steps. This procedure of comparing peaks is similar to the detection of peaks from each rotated fault-slip dataset: consequently, several maxima of peaks could be found among the backtilting steps.

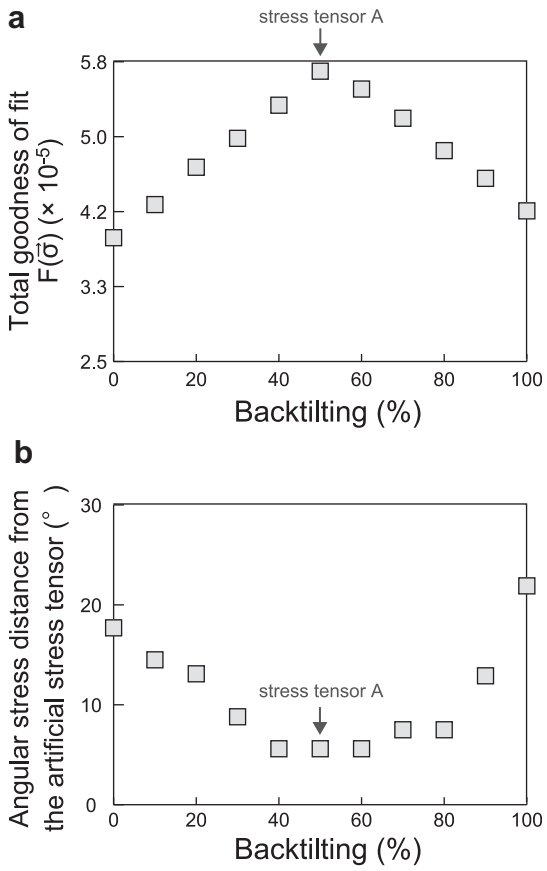

Fig. 4. Variations in the peaks of $F(\vec{\sigma})$ throughout backtilting for the fault-slip dataset of Case 1. (a) Peak values of $F(\vec{\sigma})$. (b) Angular stress distances of peaks from the artificial stress tensor.

For backtilting, fault-slip datasets were rotated using the software 'KUT' (Tomita and Yamaji, 2003). The HIM software used in this paper was written by the second author and is available at http://www.kueps.kyoto-u.ac.jp/web-bs/k_sato/.

3. Application of the method to artificial datasets

To assess the validity of the proposed incremental fold test for HIM, we applied the method to two different artificial fault-slip datasets prepared based on the Wallace–Bott hypothesis. We assumed that faults were observed in folded strata with limb dips of up to 45°, for folds with a N–S-trending horizontal hinge line and with a vertical axial plane.

3.1. Case 1: homogeneous dataset for syn-fold faulting

In the first case, we assumed that faulting occurred in the middle of folding within a uniform stress regime. We prepared a fault-slip dataset related to fault activity triggered by a compressional stress tensor characterized by a σ_1 axis oriented E–W, a σ_3 axis oriented vertical, $\Phi = 0.5$, and for the time when limb dips were 50% of the final values. Sixty fault-slip data with randomly oriented fault normals (20 full data, 20 line-only data, and 20 sense-only data) were assumed to have been observed. Half of the data (i.e., 10 full data, 10 line-only data, and 10 sense-only data) were collected from the limb dipping to the east at an angle of up to 45°, and the other data were collected from the limb dipping to the west at up to 45° (left-hand column in Fig. 3).

The artificial dataset was backtilted stepwise about the bedding planes associated with each fault, with each step representing 10% of the total tilt. Each of the rotated fault-slip datasets was then processed by HIM. Fig. 3 shows tangent–lineation diagrams (Twiss and Gefell, 1990) and the visualized $F(\vec{\sigma})$ of HIM for the fault-slip datasets with backtilting amount of 0, 50, and 100%. Paired stereograms (center and right-hand columns in Fig. 3) show the principal axes and Φ of reduced stress tensors, which have relatively high values of $F(\vec{\sigma})$ for each dataset shown in the figure.

Fig. 4 shows variations in the peaks of $F(\vec{\sigma})$ versus backtilting. The peaks correspond to the potential solutions of HIM for each dataset. After comparing the peaks among the different steps, a single maximum of $F(\vec{\sigma})$ was clearly found, which is referred to as stress tensor *A* (Fig. 4a). Stress tensor *A* is a reverse-faulting stress tensor with σ_1 oriented E–W, and characterized by an intermediate stress ratio at 50% backtilting, which is comparable to the artificial stress tensor assumed in the model (Fig. 3). To investigate the degree of similarity between the detected reduced stress tensor and the artificial stress tensor, we calculated the angular stress distances (Yamaji and Sato, 2006) between them. The angular stress differences of potential solutions from the artificial stress tensor are minimized for stress tensor A (Fig. 4b), which means that stress tensor A is the closest to the artificial stress tensor among the potential solutions. Consequently, the proposed method succeeded

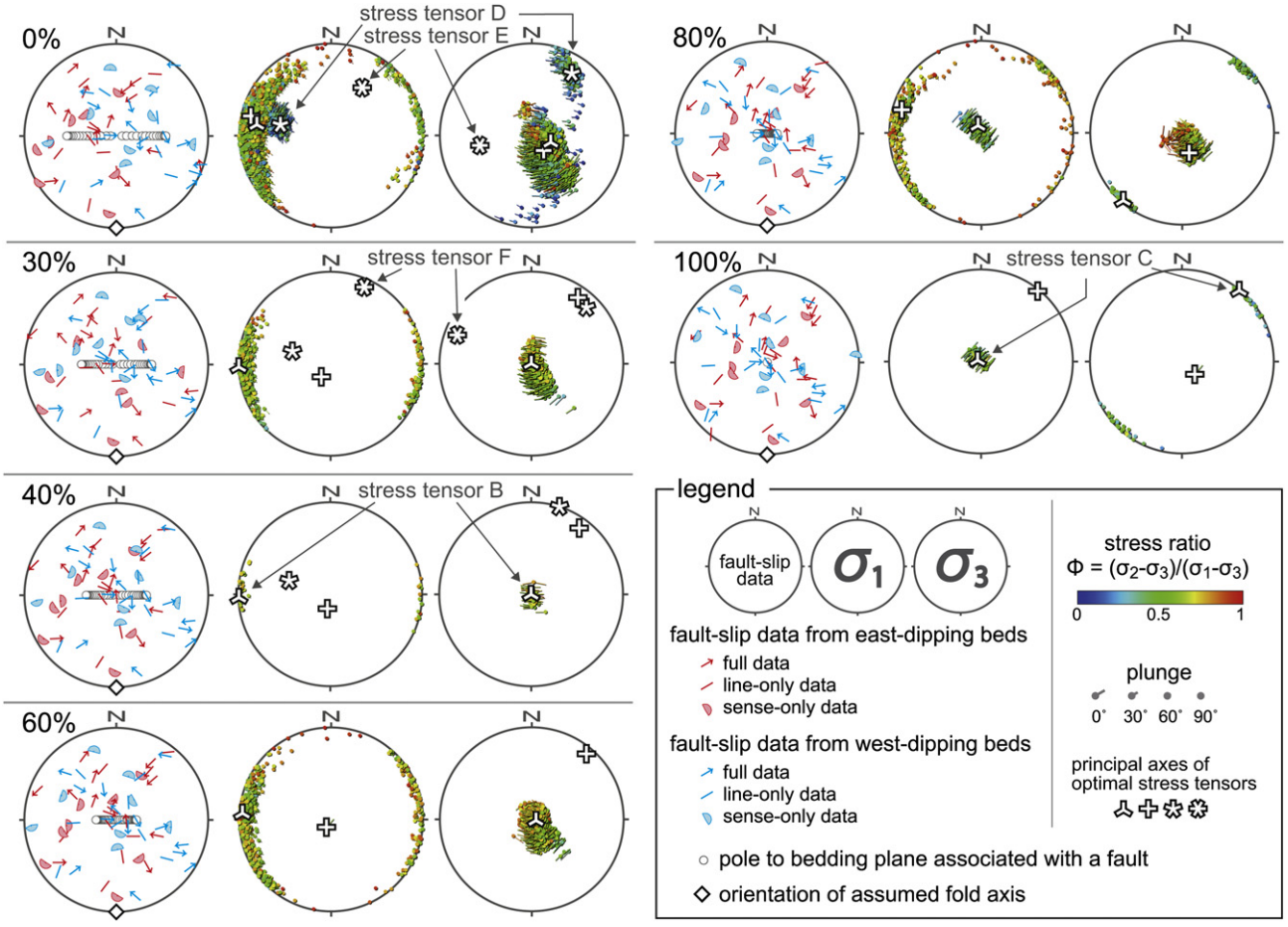

Fig. 5. Stereograms showing the artificial fault-slip data (left-hand column) and the HIM results (center and right-hand columns) for Case 2. Lower-hemisphere, equal-area projections. Open circles in the left-hand column indicate the orientations of strata near each fault-slip data point. The fault-slip data are shown in the same column as tangent–lineation diagrams (Twiss and Gefell, 1990).

in recovering the artificial stress tensor and in determining the relative ages of folding and faulting for Case 1.

3.2. Case 2: heterogeneous dataset from faulting events of different ages

The second case assumes a rock mass subjected to two different stress tensors at different times. The first artificial stress tensor is a normal-faulting stress tensor with σ_3 oriented NE–SW (σ_1-axis: 090°/90°, σ_3-axis: 040°/00°, $\Phi = 0.6$). The other tensor is a reverse-faulting stress tensor with σ_1 oriented E–W (σ_1-axis: 270°/00°, σ_3-axis: 090°/90°, $\Phi = 0.7$). The angular stress distance between these artificial stress tensors is 138°. Sixty faults with randomly oriented fault normals were prepared based on the Wallace–Bott hypothesis. Among them, 30 faults were assumed to have been activated before folding, as a consequence of the normal-faulting stress tensor. The remaining faults were assumed to have been activated by the reverse-faulting stress tensor, when the beds were inclined at 40% of the final dips.

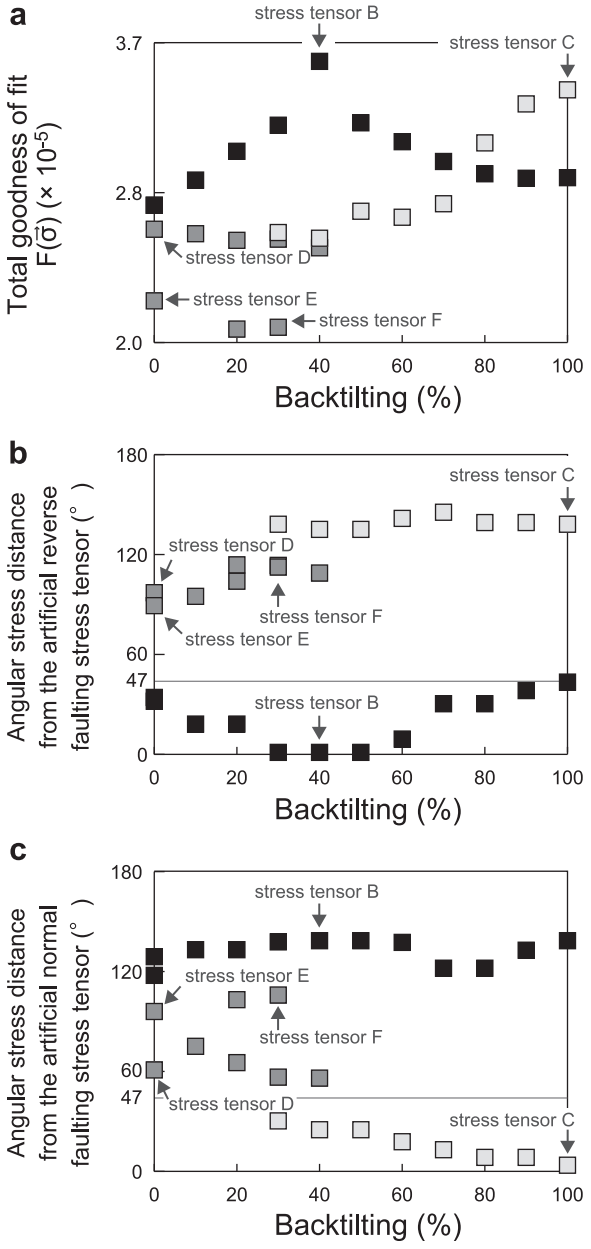

Fig. 6. Variations in the peaks of $F(\vec{\sigma})$ throughout backtilting for the fault-slip dataset of Case 2. Black (light gray) symbols represent peaks for which the angular stress distance from the artificial reverse-faulting (normal-faulting) stress tensor is 47° or less. Dark gray symbols represent peaks for which the angular stress distance from the two artificial stresses tensor is greater than 47°. (a) Peak values of $F(\vec{\sigma})$. (b) Angular stress distances of the peaks from the artificial reverse-faulting stress tensor. (c) Angular stress distances of the peaks from the artificial normal-faulting stress tensor.

The artificial dataset was backtilted stepwise about the bedding plane close to every fault with 10% of the total tilt and were then processed by HIM. Fig. 5 shows the results of the calculations for fault-slip datasets with backtilting amounts of 0, 30, 40, 60, 80, and 100%. Up to four peaks in $F(\vec{\sigma})$ were detected from each fault-slip dataset.

Fig. 6 shows variations in the peaks of $F(\vec{\sigma})$ detected through backtilting. After comparing the peaks among the different steps, five maxima of peaks were found (Fig. 6a). We refer to the tensors corresponding to the maxima as stress tensors *B*–*F*, in descending order of peak values of $F(\vec{\sigma})$ (Figs. 5 and 6).

Stress tensor *B* is a reverse-faulting stress tensor with σ_1 oriented E–W and a relatively high stress ratio at 40% backtilting (Fig. 5), comparable to the artificial reverse-faulting stress tensor. The angular stress distance between stress tensor *B* and the artificial reverse-faulting stress tensor is 1.2°, representing the ideal minimum among all potential solutions corresponding to peaks of $F(\vec{\sigma})$ (Fig. 6b).

Stress tensor *C* is a normal-faulting stress tensor with σ_3 oriented NE–SW and an intermediate stress ratio at 100% backtilting (Fig. 5), comparable to the artificial normal-faulting stress tensor. The angular stress distance between stress tensor *C* and the artificial normal-faulting stress tensor is 3.7°, representing the ideal minimum among all potential solutions corresponding to peaks of $F(\vec{\sigma})$ (Fig. 6c).

Stress tensor *D* is a reverse-faulting stress tensor with σ_1 oriented E–W and a relatively low stress ratio detected at 0% backtilting (Figs. 5 and 6 a). The angular stress distance between stress tensor *D* and the two artificial stress tensors is greater than 60° (Fig. 6b and c).

For stress tensor E, which is also detected at 0% of backtilting, σ_1 and σ_3 are oriented at 033°/38° and 259°/42°, respectively, and the stress ratio is high (Fig. 5). The angular stress distance between stress tensor *E* and the two artificial stress tensors is greater than 80° (Fig. 6b and c).

For stress tensor F, which is detected at 30% of backtilting, σ_1 and σ_3 are oriented at 024°/10° and 291°/15°, respectively, and the stress ratio is relatively high (Fig. 5). The angular stress distance between stress tensor F and the two artificial stress tensors is greater than 100° (Fig. 6b and c).

Stress tensors *B* and *C* are significant stress tensors because they are comparable to the artificial stress tensors, whereas stress tensors *D*–*F* are unexpected. Yamaji et al. (2006) reported that all inverse methods could yield unexpected stresses from a heterogeneous dataset because of the geometrical formulation of each fault-slip datum.

Although their detection is unavoidable, given the methodological limitations, there are some differences between the significant and unexpected stress tensors. First, the peak values of $F(\vec{\sigma})$ for the significant stress tensors (*B* and *C*) are much higher than those for the unexpected stress tensors (*D*–*F*) (Fig. 6a). Second, the significant stress tensors have many 'similar' peaks throughout backtilting. In this paper, we regard two reduced stress tensors of the peaks of $F(\vec{\sigma})$ to be similar if the angular stress distance between them is less than 47° based on the criterion of peak detection. Stress tensors *B* and *C* have similar peaks over a wide range of backtilting, whereas stress tensors *D*–*F* have similar peaks over a range of backtilting that is less than 20% (Fig. 6b and c). These characteristics are sufficient in terms of identifying and excluding unexpected tensors. As a result, we conclude that the proposed method was successfully applied in Case 2.

4. Application to a natural dataset

4.1. Geological setting

We applied the present method to a natural fault-slip dataset collected from Paleogene strata in the Amakusa–Kamishima area, Kyushu, southwest Japan (Fig. 7). The sedimentary basin that houses the strata was formed in the early Middle Eocene (Okada, 1992; Aita et al., 1997) and was folded during the Early Miocene (Sakai, 1993).

In this area, Paleogene strata unconformably overlie Upper Cretaceous shallow-marine sedimentary strata (Nagao, 1926; Komatsu et al., 2008), and are at least 2700 m thick (Miki and Suzukawa, 1980). The basal unit of the Paleogene strata is 40–150 m thick and consists mainly of conglomerate and reddish mudstone deposited in a fluvial environment (Miki and Matsueda, 1974; Takai and Sato, 1982). The Paleogene strata are dominated by sandstone, alternating layers of sandstone and mudstone, dark gray mudstone that contains fossil molluscs, and local coal layers (Fukuta, 1962; Mizuno, 1963; Miki, 1975; Miki and Suzukawa, 1980).

Foraminifera, radiolarian, and calcareous nannofossils indicate an early Middle Eocene age, corresponding to the P11–P12 subzones and CP12–CP15b subzones (Tashiro et al., 1980; Okada, 1992; Aita et al., 1997). The fossils of an herbivorous mammal (Tillodontia), which indicate a Paleocene–Eocene age, have been reported from the northeastern part of the study area (Miyata and Tomida, 1998).

The strata are folded about NE–SW-trending axes (Fig. 7) and dip at up to 60°. NW–SE and NNE–SSW trending faults are observed at the map scale (Fig. 7), some of which displace the adjacent strata by more than 20 m and are marked by damage zones of several meters in thickness.

4.2. Data

We collected 71 fault-slip data from minor faults within Paleogene strata with displacements of 0.2–1.0 m (Fig. 7). The in situ

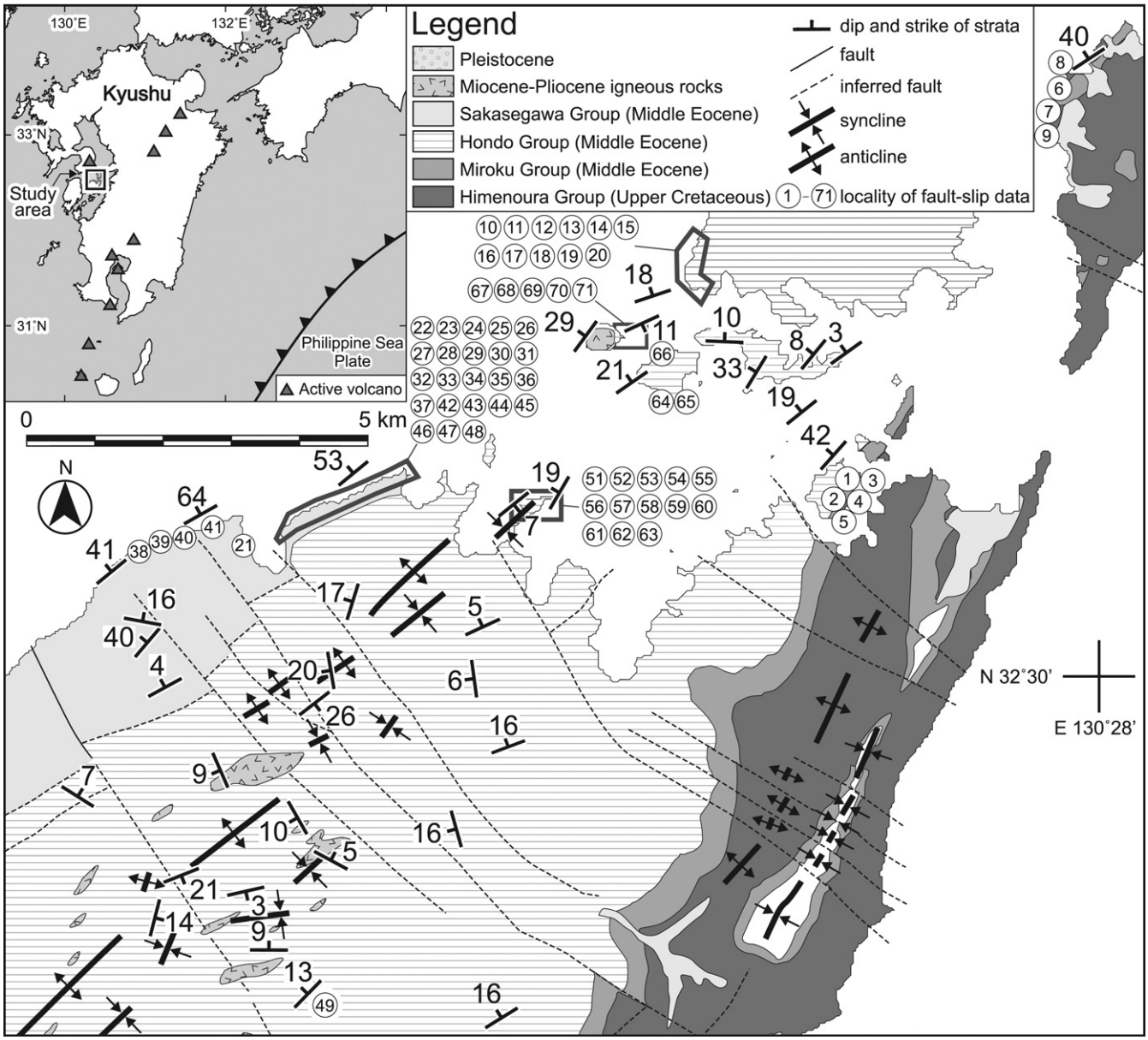

Fig. 7. Geologic map of the Amakusa–Kamishima area (after Miki, 1981).

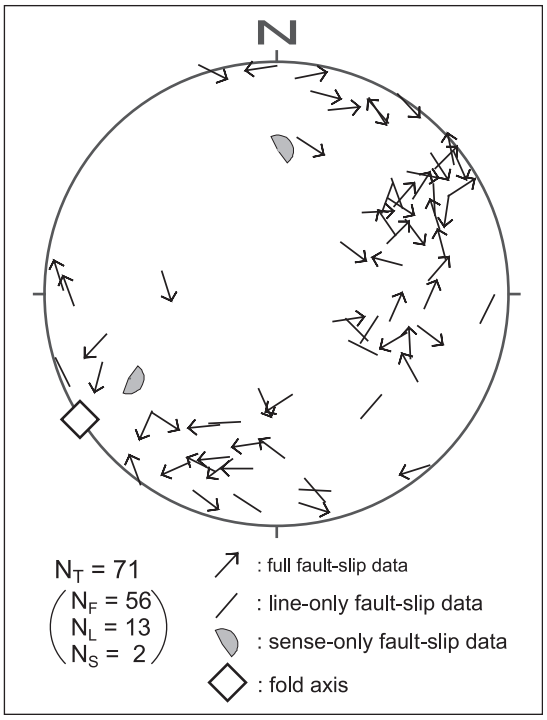

Fig. 8. Tangent-lineation diagram of in situ fault-slip data from the Amakusa–Kamishima area. Lower-hemisphere, equal-area projection. Abbreviations: N_T, number of total fault-slip data; N_F, number of full fault-slip data; N_L, number of line-only fault-slip data; N_S, number of sense-only fault-slip data.

fault-slip data are shown in Fig. 8 and referred to as the fault-slip dataset with 0% backtilting. The faults are oriented oblique to or sub-perpendicular to the fold axes. Oblique normal and strike-slip faults are dominant (Fig. 8), and about half of the faults have calcite or quartz slickenfibers. Five of the observed faults have two sets of slickenlines. In such cases, the two sets of slickenlines were treated as two sets of distinct fault-slip data. These observations indicate that the fault-slip dataset is heterogeneous; however, few features provide clues to the relative ages of activity upon these minor faults. Given these complexities, the fault-slip data could not be classified based on field observations.

4.3. Results

The fault-slip dataset obtained from observed faults in the Amakusa–Kamishima area was stepwise backtilted about bedding planes at each fault (at steps of 10%) and processed by HIM. Fig. 9 shows the results of the calculations for fault-slip datasets with backtilting amounts of 0, 10, 30, 50, 70, and 100%. Up to three peaks of $F(\overline{\sigma})$ were recognized in each fault-slip dataset. After comparing the peaks among each step, three tensors were detected as the maxima of peaks (Fig. 10a). We refer to these tensors as stress tensors *G*–*I*, in descending order of peak values of $F(\overline{\sigma})$ (Fig. 9).

Stress tensor *G* is a strike-slip faulting stress tensor with σ_1 oriented NW–SE and a relatively high stress ratio (Fig. 9). The maximum of $F(\overline{\sigma})$ corresponding to the tensor was detected at 10% and 20% of backtilting, and has the largest value in the parameter space among peaks throughout the backtilting (Fig. 10 a). Peaks similar to stress tensor *G* are recognized from 0% to 70% of backtilting (Fig. 10b).

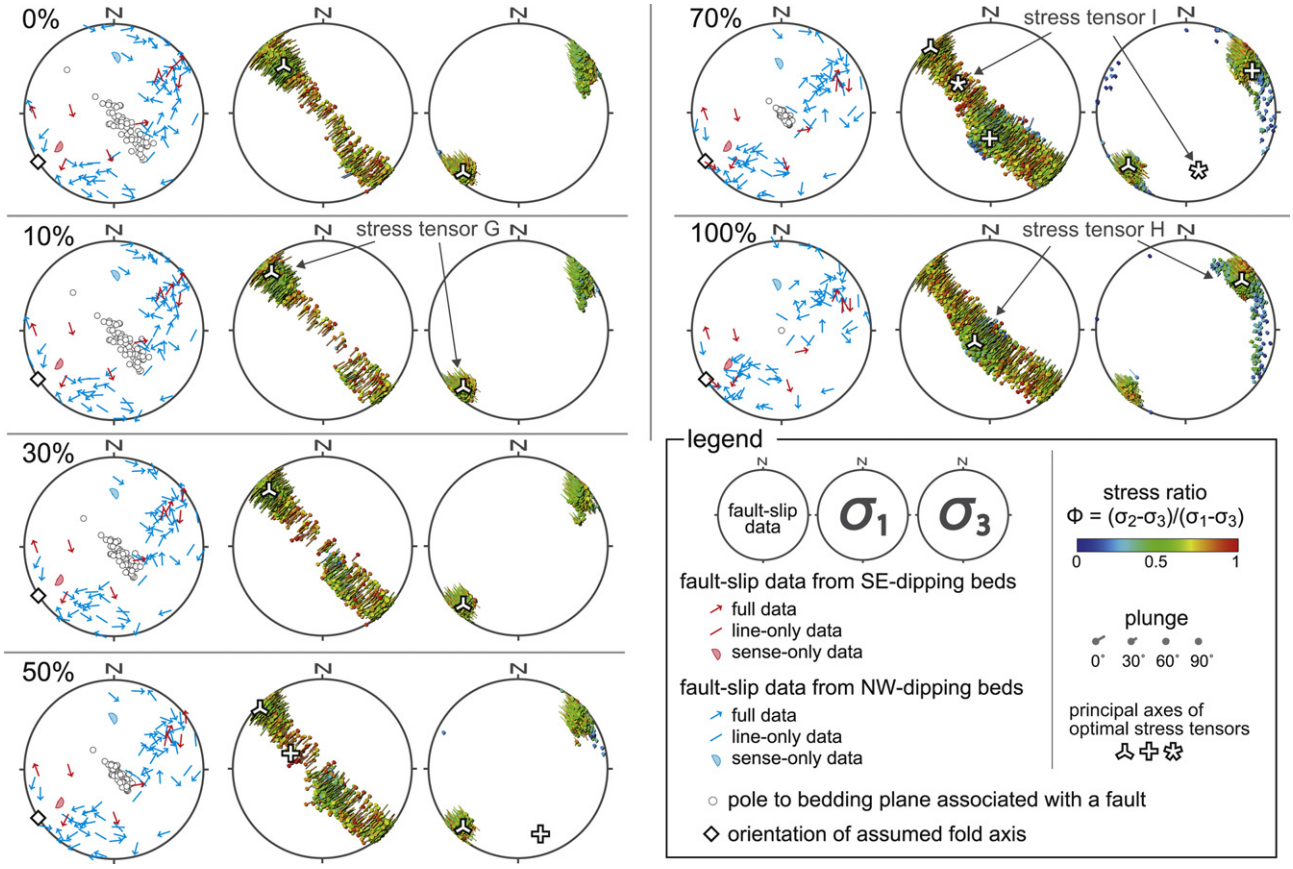

Fig. 9. Stereograms showing fault-slip data from the Amakusa–Kamishima area (left-hand column) and the results of HIM. Lower-hemisphere, equal-area projections. Open circles in the left-hand column indicate the orientation of strata near each fault-slip data point. The fault-slip data are shown in the same column as tangent–lineation diagrams. Percentage values in the upper left corner of each panel indicate the amount of backtilting.

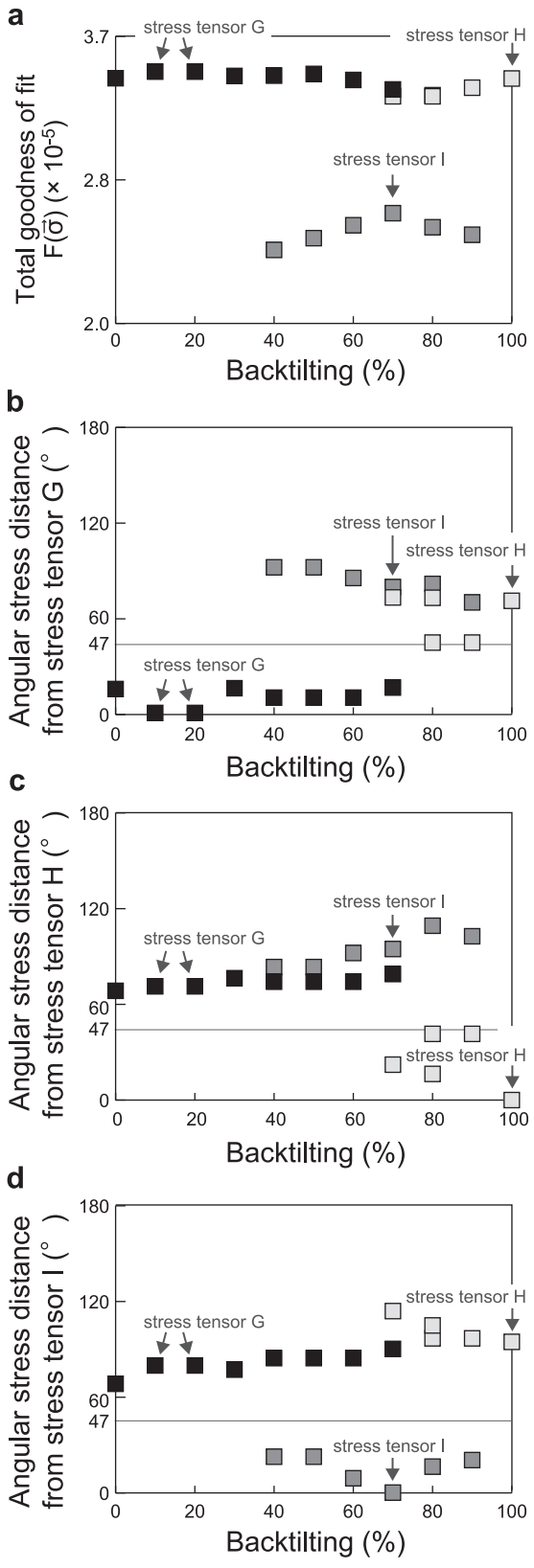

Fig. 10. Variations in the peaks of $F(\vec{\sigma})$ throughout backtilting for a fault-slip dataset from the Amakusa–Kamishima area. Black, light gray, and dark gray symbols represent peaks for which the angular stress distances from stress tensors *G*–*I* are 47° or smaller, respectively. (a) Peak values of $F(\vec{\sigma})$. (b) Angular stress distances of peaks from stress tensor *G*. (c) Angular stress distances of peaks from stress tensor *H*. (d) Angular stress distances of peaks from stress tensor *I*.

Stress tensor *H* is a normal-faulting stress tensor with σ_3 oriented NE–SW and an intermediate stress ratio of $\Phi \approx 0.4$ (Fig. 9). The maximum of $F(\vec{\sigma})$ corresponding to the tensor was detected at 100% of backtilting (Fig. 10a). Peaks similar to stress tensor *H* are recognized from 70% to 90% of backtilting (Fig. 10c).

For stress tensor *I*, σ_1 and σ_3 are oriented at around 311°/50° and 168°/34°, respectively (Fig. 9), and the tensor has a relatively high stress ratio ($\Phi = 0.7$) detected at 70% of backtilting (Fig. 10a). The peak value of stress tensor *I* in the parameter space is much smaller than the peak values for stress tensors *G* and *H* (Fig. 10a). Peaks similar to stress tensor *I* are recognized from 40% to 90% of backtilting (Fig. 10d).

The results indicate that the detected stress tensors are geologically significant, and they are necessary to explain the fault-slip data. More than 80% of the fault-slip data (59 of 71 fault-slip data) are concordant with one or more of the detected tensors, with misfit angles between the fault-slip data and the shear stress direction predicted by the detected tensors of less than 30° (Table 1). In addition, the occurrence of similar tensors corresponding to stress tensors *G*–*I* over a wide range of backtilting angles (Fig. 10b–d) supports the interpretation that they are not unexpected stress tensors that arose from a heterogeneous fault-slip dataset.

5. Discussion

5.1. Methodology

Paleostress inversion in a strongly folded rock mass is limited by a theoretical difficulty (Angelier, 1994; Yamaji et al., 2005). Several researchers have relied on the fact that one of the stress axes is oriented near-vertical at shallow levels in the crust (e.g., Martin and Bergerat, 1996; Fabbri, 2000); however, in situ stress measurements have revealed that this assumption is not always correct (Engelder, 1993; Amadei and Stephansson, 1997). In particular, the stress regime in a zone of active folding is commonly complex, and may not conform to the Anderson theory (Couples et al., 1998).

Yamaji et al. (2005) used the mean stress difference, which is the Euclidean distance to the stress difference (Orife and Lisle, 2003), to estimate the scattering of stress tensors. Yamaji et al. (2005) established a method based on a kinematic hypothesis: it was considered that the different parts of a fold kept pace with each other in terms of tilting. We adopted this assumption in the present method, although the reality is more complex than the model.

In the proposed method, we made some assumptions in order to infer the paleostresses. First, we assumed that faulting occurred episodically within limited short periods of folding, not continuously throughout the folding. Second, among the peaks of $F(\vec{\sigma})$ from each step of backtilting, we assumed the genuine stress tensor has the largest value of $F(\vec{\sigma})$ to the fault-slip dataset. We obtained satisfactory results for two artificial datasets, indicating that these assumptions are valid.

Another problem is determining the time range of faulting. In the present method, using an artificial dataset, we assumed that faulting related to each of the three artificial stress tensors occurred simultaneously; however, syn-fold faulting may occur over a relatively long time period during folding. In such a case, the fault-slip dataset probably yields a weaker peak in values of $F(\vec{\sigma})$ against backtilting. In applying the proposed model to a natural fault-slip dataset from the Amakusa–Kamishima area, we found only a minor difference between the peak values of stress tensors *G* and similar peaks (Fig. 10). This result may be attributed to the fact that faulting associated with stress tensors *G* occurred over a long period range during the later stages of folding.

Table 1
Misfit angles (d) of fault-slip data from the Amakusa–Kamishima area for stress tensors G–I. Misfit angles smaller than 30° are shaded. The locations of the fault-slip data are shown in Fig. 7. Abbreviations: F, full fault-slip data; L, line-only fault-slip data; S, sense-only fault-slip data; N, normal shear sense; R, reverse shear sense; D, dextral shear sense; S, sinistral shear sense; U, unknown shear sense.

Locality	Type	Fault plane (°)		Slickenline (°)		Sense	Misfit angles (°)		
		Dip direction	Dip	Dip direction	Dip		Stress tensor G	Stress tensor H	Stress tensor I
1	F	230	87	143	47	S	150.3	28.8	19.9
2	F	164	89	76	62	R	0.9	152.9	84.0
3	F	261	60	209	47	N	12.7	99.6	23.1
4	L	274	80	191	34	U	30.3	12.8	25.9
5	F	95	84	181	35	D	129.5	8.6	146.6
6	F	200	74	278	36	D	64.7	87.7	2.9
7	F	189	85	276	33	D	79.8	98.6	7.4
8	F	24	69	296	6	D	37.0	151.2	17.5
9	F	231	83	208	82	N	104.4	14.6	13.6
10	F	253	63	164	3	S	33.4	171.9	39.6
11	F	237	47	326	2	S	80.5	154.9	81.1
12	F	231	47	272	39	D	34.4	18.4	31.5
13	F	235	55	308	22	D	71.7	15.7	73.8
14	F	41	62	127	8	S	113.0	9.0	105.8
15	F	285	58	315	54	D	93.5	89.6	107.6
16	F	246	55	328	12	D	130.9	8.4	106.7
17	F	241	31	307	14	D	77.1	15.9	71.2
18	F	253	41	289	35	S	120.5	131.9	117.4
19	F	209	79	125	30	S	173.6	16.0	100.2
20	F	231	70	299	46	N	10.3	81.7	49.9
21	F	299	55	340	47	R	67.8	173.1	17.1
22	F	235	86	147	23	D	16.2	161.0	153.5
23	F	232	78	143	7	D	20.9	175.2	116.8
24	F	215	89	125	24	D	2.4	156.5	76.3
25	F	194	77	104	0	D	30.9	144.2	34.2
26	F	359	39	59	22	D	7.8	80.3	15.6
27	L	349	75	265	22	U	79.5	45.6	6.3
28	L	349	75	295	65	U	52.9	2.5	53.7
29	F	2	56	300	34	D	81.1	166.9	48.8
30	F	270	56	196	23	S	6.3	119.2	4.1
31	F	13	66	95	17	D	15.7	120.4	14.7
32	F	18	68	71	56	D	27.6	79.7	57.5
33	F	350	83	266	41	N	83.5	10.9	158.0
34	L	302	36	297	36	U	80.5	37.6	17.4
35	F	19	83	293	30	N	112.7	3.8	168.1
36	F	11	56	86	21	D	2.2	99.6	8.0
37	F	21	65	94	32	D	5.8	117.2	22.3
38	L	320	53	43	10	U	28.8	48.9	52.6
39	F	29	55	90	34	D	1.2	101.9	7.3
40	F	290	51	1	22	S	53.6	173.0	14.3
41	F	292	45	235	28	D	158.4	84.3	110.4
42	F	193	55	118	20	D	33.2	149.5	64.8
43	F	276	43	201	13	S	4.2	88.5	0.4
44	F	209	79	128	40	D	12.2	141.6	89.5
45	F	176	87	266	8	S	115.3	2.1	166.1
46	F	65	74	354	49	N	71.1	4.4	40.5
47	L	8	80	286	38	U	79.9	27.7	25.2
48	F	74	70	24	61	N	29.9	23.3	58.0
49	F	243	65	159	13	S	42.8	113.4	44.1
50	S	181	52	252	23	N	0.0	0.0	0.0
51	F	45	69	11	65	N	10.9	92.0	1.0
52	S	60	62	138	21	N	180.0	0.0	0.0
53	F	233	67	200	63	N	6.0	43.8	2.9
54	F	244	70	174	43	R	165.2	5.0	174.1
55	L	291	35	212	8	U	31.3	36.8	62.4
56	L	294	31	318	29	U	68.0	38.7	20.9
57	F	289	27	261	24	N	0.2	92.3	156.0
58	F	322	86	235	36	D	146.2	22.7	7.2
59	F	243	49	222	47	N	5.7	80.4	8.5
60	F	232	59	218	58	N	6.3	9.0	0.5
61	L	22	50	93	21	U	39.1	59.1	14.3
62	F	39	87	312	48	D	114.7	113.2	6.4
63	F	30	76	92	62	N	2.8	130.8	71.0
64	L	239	68	166	36	U	29.8	52.7	24.1
65	F	240	81	227	81	N	45.9	48.5	40.9
66	L	70	88	160	14	U	80.2	50.6	1.5
67	F	94	39	165	14	S	103.1	3.5	33.7
68	F	6	39	331	34	N	3.8	19.6	90.6
69	F	91	79	173	35	D	81.2	97.8	147.6
70	L	229	53	193	47	U	19.6	38.7	24.3
71	L	230	57	154	21	U	47.9	13.4	61.9

Given the above results, the proposed method is considered to be applicable to fault sets for which the relative chronology between folding and faulting cannot be determined from field observation. The proposed method could be also effective in analyzing spatial and temporal variations in the stress regime within a zone of folding. As well as for folded zones, the proposed method may be useful for regions where strata are tilted except for homocline.

5.2. Tectonic implications

Based on an analysis of fault-slip data from early Middle Eocene strata in the Amakusa–Kamishima area using the proposed method, we detected three significant reduced stress tensors corresponding to maxima of peaks of $F(\vec{\sigma})$ (stress tensors *G*–*I*). We further identified stress tensor *H* as a pre-folding stress regime, and stress tensors *G* and *I* as syn-folding stress regimes (Fig. 10). Below, we consider the relationships between these detected tensors and the tectonic settings of study area.

Stress tensor *H*, which is a normal-faulting stress tensor with σ_3 oriented NE–SW, was detected from the fault-slip dataset backtilted until the bedding plane became horizontal (Fig. 9). The result shows that the Paleogene strata in the study area experienced extensional deformation before folding. There are several Paleogene sedimentary basins in northwest Kyushu, including the present study area, and some of them are characterized by extensional structures (Sakai, 1993; Tonai et al., 2011). We consider that extensional deformation may have occurred regionally, affecting all the Paleogene sedimentary basins of northwest Kyushu (Sakai, 1993); stress tensor H in the study area is attributed to this event.

For stress tensor *I*, σ_1 and σ_3 are oriented at around 311°/50° and 168°/34°, respectively, and resulted in faulting during the early stages of folding (Fig. 9). The orientations of σ_1 and σ_3 are highly oblique to the horizontal plane (Fig. 9). The orientation of σ_2 is nearly horizontal (065°/18°) and is approximately parallel to fold axes in the study area (Figs. 7 and 8). A typical assumption made in previous studies is that brittle fault sets were formed close to the earth's surface, because according to Anderson theory, all of the principal stress axes should be either horizontal or vertical; however, the present method detected a non-Andersonian stress regime during folding. Such stress regimes at depth are caused by, for example, lateral density variations or other changes in rock properties (Sperner and Zweigel, 2010). The stress regime in a folded rock mass shows spatial and temporal variations, as indicated by field observations (Mynatt et al., 2009) and numerical experiments (Couples et al., 1998). The stress field in such a folded rock mass is heterogeneous and tends to be non-Andersonian (Couples et al., 1998, 2007).

Stress tensor *G* is a NW–SE compressional strike-slip faulting stress tensor that led to faulting during the middle to late stages of folding (Fig. 9). This stress regime appears to be discordant with folding in the study area, because the folding of sedimentary strata causes horizontal shortening and vertical extension; such a strain geometry is consistent with a reverse-faulting stress regime. Therefore, stress tensor *G* may be a local stress regime rather than the regional stress regime that produced the fold belt in the study area.

Complex three-dimensional deformation is a common feature of folding. For example, Yamaji et al. (2005) reported two different paleostress systems during folding, based on an analysis of a dataset from minor faults in a Quaternary fold belt in northeast Japan, employing the multiple-inverse method, a paleostress inversion technique (Yamaji, 2000). Both stress regimes were discordant with the strain associated with folding, and were interpreted as secondary stress regimes related to flexural slip folding. Complex fracturing during the late stages of folding has been reported from Triassic shale, sandstone, and limestone strata in southeast Utah, USA (Mynatt et al., 2009). This complexity is attributed to a spatially and temporally varying stress field. Although the amount of strain parallel to the fold axis is small relative to that oriented normal to the axis, it is possibly recorded by minor faults and detected by paleostress inversion techniques.

6. Summary

We proposed an incremental fold test for the paleostress inversion technique based on the Hough transform. The method detects significant stress tensors by simply comparing peak values of total goodness of fit and the stress differences among peaks detected from each step of backtilting of a fault-slip dataset. Application of the method using an artificial dataset revealed that it performs well for both homogeneous and heterogeneous datasets.

The proposed method was applied to a natural fault-slip dataset obtained from Paleogene strata in the Amakusa–Kamishima area, revealing three significant stress regimes: a normal-faulting stress regime that occurred before folding, and two syn-folding stresses regimes, indicating the existence of a spatially and temporally varying stress field during folding.

The present method was validated by the results of experiments using artificial and natural fault-slip datasets, indicating that this approach is applicable to fault-slip data in the case that the relative ages of folding and faulting cannot be determined based on outcrop observations. This method is probably also applicable to investigations of spatial and temporal variations of the stress field in any parts of the brittle crust where strata are tilted.

Acknowledgments

We would like to thank Hidekazu Tokuyama, Atsushi Yamaji, Masaaki Shirai, Shoichi Kiyokawa, and Hisashi Oiwane for their helpful comments and discussions. Constructive reviews by Joao Hippertt, Richard J. Lisle, and an anonymous reviewer helped to improve the manuscript. This study was supported in part by grants 20-5835 and 21740364 from JSPS.

Appendix. A.

In the present study, we use fitness functions for a full datum

$$f_F(\vec{\sigma}) \propto \begin{cases} \frac{1}{\lambda}\left(1-\frac{d}{d_T}\right) & 0^\circ \le d \le d_T \\ 0 & \text{otherwise}, \end{cases} \tag{A.1}$$

for a line-only datum we use

$$f_L(\vec{\sigma}) \propto \begin{cases} \frac{1}{\lambda}\left(1-\frac{d}{d_T}\right) & 0^\circ \le d \le d_T \\ 0 & d_T \le d \le 180^\circ - d_T \\ \frac{1}{\lambda}\left(1-\frac{180^\circ - d}{d_T}\right) & 180^\circ - d_T \le d \le 180^\circ, \end{cases} \tag{A.2}$$

and for a sense-only datum we use

$$f_S(\vec{\sigma}) \propto \begin{cases} \frac{1}{\lambda} & 0^\circ \le d \le 90^\circ \\ 0 & \text{otherwise} \end{cases} \tag{A.3}$$

where the subscripts *F*, *L*, and *S* indicate fitness functions for a full, line-only, and sense-only datum, respectively. The threshold d_T is

set to 60° in this paper, and λ is the normalizing factor used to satisfy

$$\int_{S_5} f_*(\vec{\sigma})\mathrm{d}S = 1, \tag{A.4}$$

where * is the wildcard standing for one of *F*, *L*, or *S*, and the integration is taken over the surface of S_5. See Sato (2006) for further explanations.

References

Aita, Y., Ogata, K., Murakami, H., Shimamura, K., Sakai, T., 1997. Late Cretaceous and Eocene radiolarians from the Goshonoura and Maki-shima Islands, Amakusa, Kumamoto, Japan. News of Osaka Micropaleontologists, Special Volume 10, 267–283.

Amadei, B., Stephansson, O., 1997. Rock Stress and Its Measurement. Chapman and Hall, London.

Angelier, J., 1994. Fault slip analysis and paleostress reconstruction. In: Hancock, P. (Ed.), Continental Deformation. Pergamon Press, Oxford, pp. 53–101.

Angelier, J., Barrier, E., Chu, H.T., 1986. Plate collision and paleostress trajectories in a fold-thrust belt: the foothills of Taiwan. Tectonophysics 125, 161–178. doi:10.1016/0040-1951(86)90012-0.

Armijo, R., Carey, E., Cisternas, A., 1982. The inverse problem in microtectonics and the separation of tectonic phases. Tectonophysics 82, 145–160. doi:10.1016/0040-1951(82)90092-0.

Bott, M.H.P., 1959. The mechanics of oblique slip faulting. Geological Magazine 96, 109–117. doi:10.1017/S0016756800059987.

Butler, R.F., 1992. Paleomagnetism: Magnetic Domains to Geologic Terrains. Blackwell Scientific Publisher, Boston.

Choi, P.Y., Kwon, S.K., Hwang, J.H., Lee, S.R., An, G.O., 2001. Paleostress analysis of the Pohang-Ulsan area, Southeast Korea: tectonic sequence and timing of block rotation. Geosciences Journal 5, 1–18. doi:10.1007/BF02910169.

Couples, G.D., Lewis, H., Olden, P., Workman, G.H., Higgs, H.N., 2007. Insights into the Faulting Process from Numerical Simulations of Rock-layer Bending. In: Geological Society, London, Special Publications, vol. 289 doi:10.1144/SP289.10161–186.

Couples, G.D., Lewis, H., Tanner, P.W.G., 1998. Strain Partitioning during Flexural-slip Folding. In: Geological Society, London, Special Publications, vol. 127 doi:10.1144/GSL.SP.1998.127.01.12149–165.

Engelder, T., 1993. Stress Regimes in the Lithosphere. Princeton University Press, Princeton.

Etchecopar, A., Vasseur, G., Daignieres, M., 1981. An inverse problem in microtectonics for the determination of stress tensors from fault striation analysis. Journal of Structural Geology 3, 51–65. doi:10.1016/0191-8141(81)90056-0.

Fabbri, O., 2000. Extensional deformation in the northern Ryukyu arc indicated by mesoscale fractures in the middle Miocene deposits of Tanegashima Island, Japan. Journal of the Geological Society of Japan 106, 234–243.

Fry, N., 1999. Striated faults: visual appreciation of their constraint on possible paleostress tensors. Journal of Structural Geology 21, 7–21. doi:10.1016/S0191-8141(98)00099-6.

Fry, N., 2001. Stress space: striated faults, deformation twins, and their constraints on paleostress. Journal of Structural Geology 23, 1–9. doi:10.1016/S0191-8141(00)00136-X.

Fukuta, O., 1962. Eocene Foraminifera from the Kyoragi beds in Shimo-shima, Amakusa Islands, Kumamoto Prefecture, Kyushu, Japan. Reports. Geological Survey of Japan 194, 1–31.

Graham, J.W., 1949. The stability and signigicance of magnetism in sedimentary rocks. Journal of Geophysical Research 54, 131–167. doi:10.1029/JZ054i002p00131.

Komatsu, T., Ono, M., Naruse, H., Kumagae, T., 2008. Upper Cretaceous depositional environments and bivalve assemblages of far-east Asia: the Himenoura Group, Kyushu, Japan. Cretaceous Research 29, 489–508. doi:10.1016/j.cretres.2007.10.001.

Lisle, R.J., Orife, T., Arlegui, L., 2001. A stress inversion method requiring only fault slip sense. Journal of Geophysical Research 106, 2281–2289. doi:10.1029/2000JB900353.

Martin, P., Bergerat, F., 1996. Palaeo-stresses inferred from macro- and micro-fractures in the Balazuc-1 borehole (GPF programme). Contribution to the tectonic evolution of the Cevennes border of the SE Basin of France. Marine and Petroleum Geology 13, 671–684. doi:10.1016/0264-8172(95)00063-1.

Miki, T., 1975. Formation and development of sedimentary basins during the Paleogene in Amakusa and its adjacent areas, Western Kyushu. Memoirs of the Faculty of Science, Kyushu University, Series D, Geology 23, 165–209.

Miki, T., 1981. Restudy of the Lowest Parts of the Paleogene Sequences in Western Kyushu, Japan. Science Reports, vol. 14. Department of Geology, Kyushu University. 63–71.

Miki, T., Matsueda, H., 1974. Akasaki Formation in Amakusa, Western Kyushu, Japan. Science Reports, vol. 12. Department of Geology, Kyushu University. 27–40.

Miki, T., Suzukawa, T., 1980. The so-called Kyoragi formation in Amakusa-Kamishima. Science Reports, vol. 13. Department of Geology, Kyushu University. 285–293.

Miyata, K., Tomida, Y., 1998. Trogosus-like tillodont (Tillodontia, Mammalia) from the early middle Eocene of Japan. Paleontological Research 2, 193–198.

Mizuno, A., 1963. Paleogene and lower Neogene biochoronology of west Japan (III. Stratigraphic and geographic distributions of molluscan faunas in west Japan). Journal of the Geological Society of Japan 69, 38–50.

Mynatt, I., Seyum, S., Pollard, D.D., 2009. Fracture initiation, development, and reactivation in folded sedimentary rocks at Raplee Ridge, UT. Journal of Structural Geology 31, 1100–1113. doi:10.1016/j.jsg.2009.06.003.

Nagao, T., 1926. Stratigraphy of the Paleogene in Kyushu (I). Journal of Geography 38, 115–130.

Nemcok, M., Lisle, R.J., 1995. A stress inversion procedure for polyphase fault/slip data sets. Journal of Structural Geology 17, 1445–1453. doi:10.1016/0191-8141(95)00040-K.

Okada, H., 1992. Calcareous nannofossils and biostratigraphy of the Paleogene sequences of the northern Kyushu, Japan. Journal of the Geological Society of Japan 98, 509–528.

Orife, T., Lisle, R.J., 2003. Numerical processing of palaeostress results. Journal of Structural Geology 25, 949–957. doi:10.1016/S0191-8141(02)00120-7.

Rossetti, F., Storti, F., Salvini, F., 2000. Cenozoic noncoaxial transtension along the western shoulder of the Ross Sea, Antarctica, and the emplacement of McMurdo dyke arrays. Terra Nova 12, 60–66. doi:10.1111/j.1365-3121.2000.00270.x.

Sakai, H., 1993. Tectonics and sedimentation of the Tertiary sedimentary basins in the northern Kyushu. Memoirs of the Geological Society of Japan 42, 183–201.

Sato, K., 2006. Incorporation of incomplete fault-slip data into stress tensor inversion. Tectonophysics 421, 319–330. doi:10.1016/j.tecto.2006.05.004.

Sato, K., Yamaji, A., 2006a. Embedding stress difference in parameter space for stress tensor inversion. Journal of Structural Geology 28, 957–971. doi:10.1016/j.jsg.2006.03.004.

Sato, K., Yamaji, A., 2006b. Uniform distribution of points on a hypersphere for improving the resolution of stress tensor inversion. Journal of Structural Geology 28, 972–979. doi:10.1016/j.jsg.2006.03.007.

Shan, Y., Li, Z., Lin, G., 2004. A stress inversion procedure for automatic recognition of polyphase fault/slip data sets. Journal of Structural Geology 26, 919–925. doi:10.1016/j.jsg.2003.10.001.

Sperner, B., Zweigel, P., 2010. A plea for more caution in fault-slip analysis. Tectonophysics 482, 29–41. doi:10.1016/j.tecto.2009.07.019.

Storti, F., Rossetti, F., Salvini, F., 2001. Structural architecture and displacement accommodation mechanisms at the termination of the Priestley Fault, northern Victoria Land, Antarctica. Tectonophysics 341, 141–161. doi:10.1016/S0040-1951(01)00198-6.

Takai, Y., Sato, H., 1982. Geology of the Oniki and Ushibuka district. Quadrangle series, scale 1:50,000. Geological Survey of Japan.

Tashiro, M., Okada, H., Taira, A., Otsuka, M., 1980. Middle Eocene calcareous nannofossils from the basal part of the Tertiary strata in Amakusa-Shimojima, Kyushu. Journal of the Geological Society of Japan 86, 139–141.

Tomita, S., Yamaji, A., 2003. KUT: software to rotate orientation data. Geoinformatics 14, 85–104.

Tonai, S., Suganuma, Y., Ashi, J., Itaya, T., Oiwane, H., Kiyokawa, S., 2011. Differential timing of vertical-axis block rotations in the northern Ryukyu Arc: paleomagnetic evidence from the Koshikijima Islands, Japan. Tectonophysics 497, 71–84. doi: 10.1016/j.tecto.2010.11.003.

Twiss, R.J., Gefell, M.J., 1990. Curved slickenfibers – a new brittle shear sense indicator with application to a sheared serpentinite. Journal of Structural Geology 12, 471–481. doi:10.1016/0191-8141(90)90035-W.

Vandycke, S., Bergerat, F., 2001. Brittle tectonic structures and palaeostress analysis in the Isle of Wight, Wessex basin, southern U.K. Journal of Structural Geology 23, 393–406. doi:10.1016/S0191-8141(00)00125-5.

Viola, G., Ganerod, G.V., Wahlgren, C.H., 2009. Unraveling 1.5 Ga of brittle deformation history in the Laxemar-Simpevarp area, southeast Sweden: a contribution to the Swedish site investigation study for the disposal of highly radioactive nuclear waste. Tectonics 28 doi:10.1029/2009TC002461.

Wallace, R.E., 1951. Geometry of shearing stress and relation of faulting. Journal of Geology 59, 118–130. doi:10.1086/625831.

Yamaji, A., 2000. The multiple inverse method: a new technique to separate stresses from heterogeneous fault-slip data. Journal of Structural Geology 22, 441–452. doi:10.1016/S0191-8141(99)00163-7.

Yamaji, A., 2003. Slab rollback suggested by latest Miocene to Pliocene forearc stress and migration of volcanic front in southern Kyushu, northern Ryukyu Arc. Tectonophysics 364, 9–24. doi:10.1016/S0040-1951(03)00047-7.

Yamaji, A., Otsubo, M., Sato, K., 2006. Paleostress analysis using the Hough transform for separating stresses from heterogeneous fault-slip data. Journal of Structural Geology 28, 980–990. doi:10.1016/j.jsg.2006.03.016.

Yamaji, A., Sato, K., 2006. Distances for the solutions of stress tensor inversion in relation to misfit angles that accompany the solutions. Geophysical Journal International 167, 933–942. doi:10.1111/j.1365-246X.2006.03188.x.

Yamaji, A., Tomita, S., Otsubo, M., 2005. Bedding tilt test for paleostress analysis. Journal of Structural Geology 27, 161–170. doi:10.1016/j.jsg.2004.08.006.

Žalohar, J., Vrabec, M., 2007. Paleostress analysis of heterogeneous fault-slip data: the Gauss method. Journal of Structural Geology 29, 1798–1810. doi:10.1016/j.jsg.2007.06.009.